Energy Proceedings
Vol 31, 2023
ISSN 2004-2965

$LiAlO_2$ Modified Lithium Metal for $Li_{10}GeP_2S_{12}$-Based All-Solid-State Lithium Batteries

Xinshuang Chang[1,2], Wei Weng[1], Mengqi Li[1], George Z. Chen[4], Kam Loon Fow[2,3*], Xiayin Yao[1*],

1 Ningbo Institute of Materials Technology and Engineering, Chinese Academy of Sciences, Ningbo 315201, P.R. China
2 Department of Chemical and Environmental Engineering, Faculty of Science and Engineering, University of Nottingham Ningbo China, Ningbo 315100, P.R. China
3 Key Laboratory of Carbonaceous Wastes Processing and Process Intensification of Zhejiang Province, University of Nottingham Ningbo China, Ningbo 315100, P.R. China
4 Department of Chemical and Environmental Engineering, Faculty of Engineering, University of Nottingham, University Park, Nottingham NG7 2RD, UK
* Corresponding Author: kam-loon.fow@nottingham.edu.cn; yaoxy@nimte.ac.cn

ABSTRACT

Lithium metal is a promising negative electrode material that has received extensive attention owing to its ultrahigh theoretical specific capacity (3860 mAh g^{-1}) and extremely low standard electrode potential (−3.04 V *vs* standard hydrogen electrode). However, the formation of lithium dendrite and the unstable interface between solid electrolyte and lithium metal have hindered the application of lithium metal in sulfide-based all-solid-state batteries. In this work, a $LiAlO_2$ interface layer is coated on the surface of lithium metal through magnetic sputtering method. As $LiAlO_2$ can function as a good Li-ion conductor but an electronic insulator, the $LiAlO_2$ interface layer can effectively suppress the severe interface reaction between lithium metal and the $Li_{10}GeP_2S_{12}$ solid electrolyte. The $Li@LiAlO_2/Li_{10}GeP_2S_{12}/Li@LiAlO_2$ symmetric cell was stably cycled for 3000 h with a low overpotential of 200 mV at 0.1 mA cm^{-2} and 0.1 mAh cm^{-2}. Moreover, unlike the rapid capacity decay of the $Li/Li_{10}GeP_2S_{12}/LiCoO_2@LiNbO_3$ full cell, the $Li@LiAlO_2/Li_{10}GeP_2S_{12}/LiCoO_2@LiNbO_3$ full cell remained stable for 96 cycles with a high reversible capacity of 115 mAh g^{-1}.

Keywords: $LiAlO_2$, lithium metal, $Li_{10}GeP_2S_{12}$, interface modification, magnetic sputtering, all-solid-state batteries

1. INTRODUCTION

Lithium-ion batteries have been widely used in portable electronic devices and electric vehicles due to their favorable energy density [1, 2]. However, the energy density of current lithium-ion batteries [3, 4] hardly meet the increasing demand for electric vehicles and grid energy storage systems, and the growth rate of energy density is only 7-8% per year [5]. One of reasons for the limited energy density is that the capacities of the current negative and positive electrode materials of lithium-ion batteries are approaching their theoretical values, especially the graphite negative electrode.

All-solid-electrolyte lithium batteries have been considered as the next-generation batteries with greatly enhanced energy density surpassing current lithium-ion batteries [6, 7]. Lithium metal is an ideal negative electrode material for lithium batteries as it exhibits ultrahigh specific capacity (3860 mAh g^{-1}), extremely low electrochemical potential (−3.04 V *vs* standard hydrogen electrode), and low density of 0.534 g cm^{-3} [8-10].

However, lithium dendrites growth and detrimental interface side reactions have seriously limited the application of lithium metal negative electrode [11]. Inorganic solid electrolytes with high mechanical strength are promising for preventing the growth of lithium dendrites [12]. Among the inorganic solid electrolytes, $Li_{10}GeP_2S_{12}$ with high ionic conductivity (1.2×10^{-2} S cm^{-1}) and excellent capability of dendrites

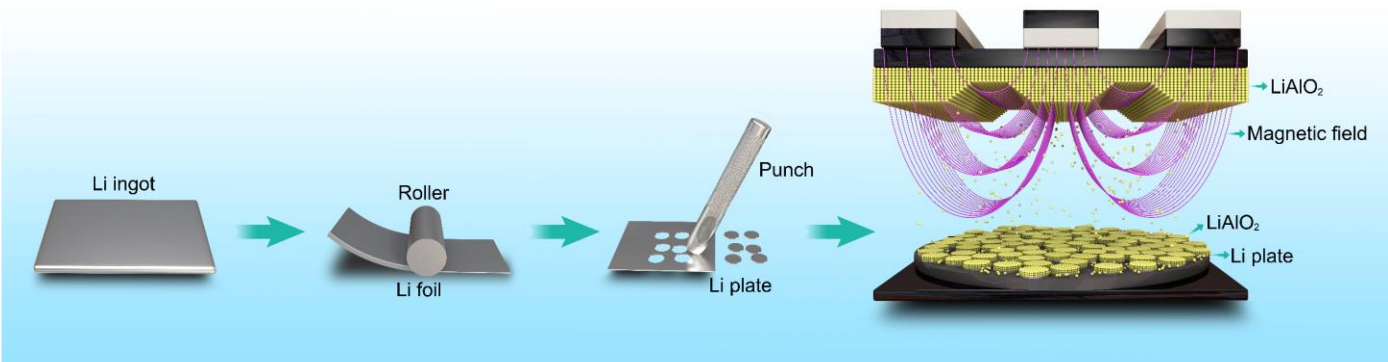

Fig. 1. Schematic illustration of preparation procedures of Li@$LiAlO_2$ electrode.

suppression has been widely studied [13, 14]. However, $Li_{10}GeP_2S_{12}$ can be easily reduced by lithium metal and the decomposition products of Li_2S, Li_3P and Ge/Li-Ge alloy with poor ion conductance continuously accumulate at the interface, which leads to large increase of the cell impedance and results in rapid cell failure [15]. Shi et al. have achieved improved interface stability by introducing an amorphous Li_3PO_4 layer at the $Li_{10}GeP_2S_{12}$/lithium metal interface [16]. In addition, alloys such as Li-Ag [17], Li-In [18] and Li-Sn [19] have also been used as a buffer layer to provide effective protection for $Li_{10}GeP_2S_{12}$. Thus, constructing a protective layer is an effective strategy to stabilize the $Li_{10}GeP_2S_{12}$/lithium metal interface.

In this work, a $LiAlO_2$ interface layer was constructed on the surface of lithium metal through radio frequency magnetic sputtering method which can fabricate uniform and dense coatings to provide effective protection for $Li_{10}GeP_2S_{12}$. In addition, the $LiAlO_2$ layer exhibits a good mechanical property and can physically isolate the direct contact between $Li_{10}GeP_2S_{12}$ and lithium metal. The $LiAlO_2$ layer can effectively suppress the decomposition of $Li_{10}GeP_2S_{12}$ resulting from reduction by lithium metal, as $LiAlO_2$ can function as a fast ionic conductor but an electronic insulator [20]. As a result, the greatly improved stability at $Li_{10}GeP_2S_{12}$/lithium metal interface is achieved. The Li@$LiAlO_2$/$Li_{10}GeP_2S_{12}$/Li@$LiAlO_2$ symmetric cell can stably cycle up to 3000 h and the Li@$LiAlO_2$/$Li_{10}GeP_2S_{12}$/$LiCoO_2$@$LiNbO_3$ full cell shows a high reversible capacity of 115 mAh g^{-1} after 96 cycles.

2. EXPERIMENT

2.1 Preparation of Li@$LiAlO_2$ electrode

The $LiAlO_2$ target material was purchased from Zhongnuo New Materials (Beijing) Technology Co., Ltd. Fig. 1 schematically illustrates the preparation procedure for the Li@$LiAlO_2$ electrode. The diameter and thickness of the Li metal plate were 10 mm and 0.5 mm, respectively. The $LiAlO_2$ layer was magnetically sputtered on the lithium plate for 12 h at a power of 50 W and a pressure of 0.5 Pa. All samples were prepared and tested in an argon-filled glove box. The magnetic sputtering (RH450) apparatus was coupled to an argon-filled glove box so that the samples were protected by inert gas before and after sputtering.

2.2 Characterization of the $LiAlO_2$ Layer

The surface morphology and element distribution of the Li@$LiAlO_2$ was characterized by scanning electron microscope (SEM， Regulus-8230, Hitachi) and energy dispersive X-ray spectroscopy (EDX), respectively. The valence state of elements on the $LiAlO_2$ layer was identified by X-ray photoelectron spectroscopy (XPS. AXIS ULTRA DLD). The test data were corrected with the standard value of 284.6 eV (C-C binding energy), and the CasaXPS software was used for peak fitting. The elastic modulus of the $LiAlO_2$ layer was measured on a scanning probe microscope (3100 SPM).

2.3 Fabrication of symmetric and full cells

Symmetric cells of Li@$LiAlO_2$/$Li_{10}GeP_2S_{12}$/Li@$LiAlO_2$ were fabricated. Specifically, 150 mg of $Li_{10}GeP_2S_{12}$ powder were compressed at 240 MPa to form the dense electrolyte layer. Then two Li@$LiAlO_2$ foils were attached on both sides of the $Li_{10}GeP_2S_{12}$ layer and compressed at 360 MPa. For full cells fabrication, the cathode was made by mixing $LiCoO_2$@$LiNbO_3$ and $Li_{10}GeP_2S_{12}$ with 70:30 weight ratio. The cathode material (3 mg) was uniformly dispersed on one side of $Li_{10}GeP_2S_{12}$ layer and compressed at 120 MPa. Subsequently the Li@$LiAlO_2$ or Li as negative electrode was attached on the other side of the $Li_{10}GeP_2S_{12}$ layer and compressed at 360 MPa. The stainless steels were used as current collectors.

2.4 Electrochemical Measurements

The electrochemical performance of Li@$LiAlO_2$/$Li_{10}GeP_2S_{12}$/$LiCoO_2$@$LiNbO_3$ full cells and

$Li@LiAlO_2/Li_{10}GeP_2S_{12}/Li@LiAlO_2$ symmetric cells were tested on a battery test system (LAND CT-2001A, Wuhan Rambo Testing Equipment Co., Ltd.). The cell impedance tests were carried out on an electrochemical workstation (1470E) from 0.01 Hz to 1 MHz with an amplitude of 15 mV at 25 ^{o}C.

3. RESULTS AND DISCUSSION

As presented in Fig. 2, the surface of lithium metal (Fig. 2a) shows an uneven morphology with evident minor cracks. Whereas the uniform surface morphology of $Li@LiAlO_2$ (Fig. 2b) and homogeneously distributed Al (Fig. 2c) and O (Fig. 2d) element demonstrate that a dense $LiAlO_2$ layer was successfully fabricated on the lithium metal through magnetic sputtering. Fig. 3 shows the XPS results of the $LiAlO_2$ layer (Fig. 3a). The peak at 530.6 eV is corresponding to the O 1s (Fig. 3b), and the peak at 55.1 eV is corresponding to the Li 1s (Fig. 3c) in the $LiAlO_2$ layer which is different to the lithium metal (55.35 eV). Also, the peak at about 74.8 eV, which is close to the binding energy of Al^{3+} in $LiAlO_2$, further confirms the existence of $LiAlO_2$ layer.

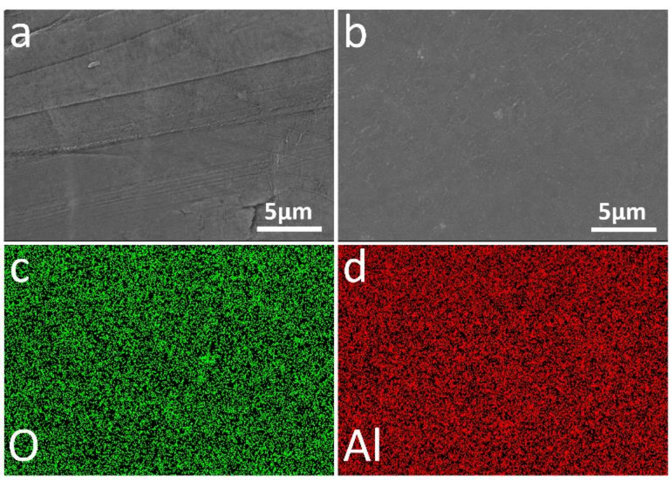

Fig. 2. SEM images of (a) Li and (b) $Li@LiAlO_2$, and the corresponding EDX elemental mapping of (c) O and (d) Al of a $Li@LiAlO_2$ sample.

Moreover, the mechanical property of the $LiAlO_2$ layer was investigated by scanning probe microscopy. As shown in Fig. 4, the surface of the $LiAlO_2$ layer (Fig. 4a) is quite flat, indicating a uniform formation of the $LiAlO_2$ layer. The high elastic modulus (Fig. 4b) concentrated between 20-50 GPa (>10 GPa of the lithium dendrite) [21] is helpful to prevent the penetration of lithium dendrites [22, 23].

To evaluate the performances of the $LiAlO_2$ layer on the $Li_{10}GeP_2S_{12}$/lithium interface, the symmetric cells $Li@LiAlO_2/Li_{10}GeP_2S_{12}/Li@LiAlO_2$ and $Li/Li_{10}GeP_2S_{12}/Li$ were assembled and tested at 0.1 mA cm^{-2} with different areal capacity. As shown in Fig. 5a, compared with rapid increase overpotential of $Li/Li_{10}GeP_2S_{12}/Li$ cell, the $Li@LiAlO_2/Li_{10}GeP_2S_{12}/Li@LiAlO_2$ cell can stably cycle up to 3000 h with a small polarization voltage of 200 mV at

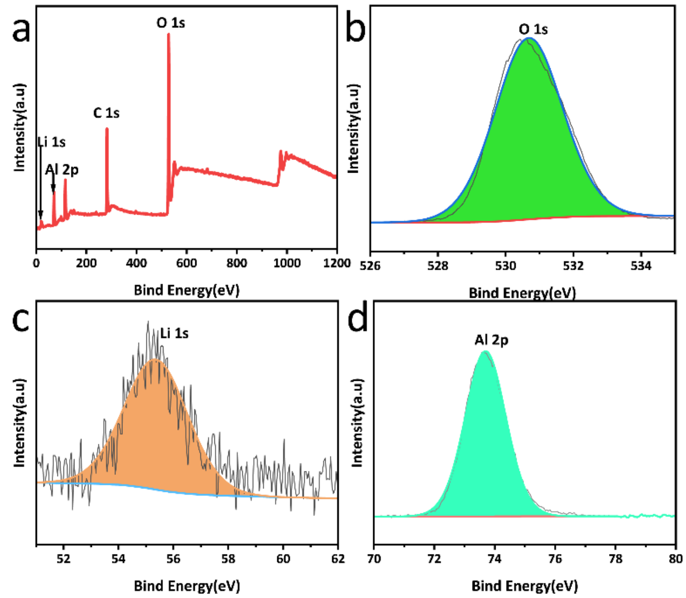

Fig. 3. XPS spectra of (a) Original XPS survey spectra. (b) O 1s, (c) Li 1s and (d) Al 2p for $Li@LiAlO_2$.

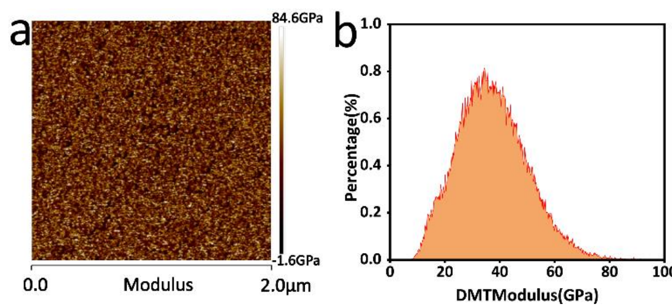

Fig. 4. (a) The morphology photo of $LiAlO_2$ layer. (b) Elastic modulus distribution of $LiAlO_2$ layer.

0.1 mA cm^{-2} and 0.1 mAh cm^{-2}. The symmetric $Li@LiAlO_2/Li_{10}GeP_2S_{12}/Li@LiAlO_2$ cells can also stably cycle up to 2000 h and 1000 h at higher areal capacities of 0.5 and 1.0 mAh cm^{-2}, respectively (Fig. 5b-c). Fig. 5d compares the rate capability of $Li@LiAlO_2/Li_{10}GeP_2S_{12}/Li@LiAlO_2$ and $Li/Li_{10}GeP_2S_{12}/Li$ symmetric cells. Compared with the higher overpotentials of $Li/Li_{10}GeP_2S_{12}/Li$ cell observed at all current densities, the overpotentials of the $Li@LiAlO_2/Li_{10}GeP_2S_{12}/Li@LiAlO_2$ cell were remarkedly lower. The $Li@LiAlO_2/Li_{10}GeP_2S_{12}/Li@LiAlO_2$ cell had a low overpotential of 43 mV at a current density of 0.1 mA cm^{-2}. Notably, the overpotential of this symmetric cell increased from 191 mV to 2134 mV when the current density was increased from 0.25 to 1.0 mA cm^{-2}. These results demonstrate that the detrimental $Li_{10}GeP_2S_{12}$/lithium metal interface side reactions can be effectively suppressed by the $LiAlO_2$ layer and the Li@$LiAlO_2$/$Li_{10}GeP_2S_{12}$/Li@$LiAlO_2$ symmetric cells show a stable cyclic stability.

Due to the good protection of the $LiAlO_2$ layer on $Li_{10}GeP_2S_{12}$/lithium metal interface, the all-solid-state lithium batteries with Li@$LiAlO_2$ as negative electrode were further investigated. Fig. 6a shows the charge and discharge curve of Li/$Li_{10}GeP_2S_{12}$/$LiCoO_2$@$LiNbO_3$ cell, showing a rapid capacity decay and large polarization voltages after 5 cycles. In comparison, the Li@$LiAlO_2$/$Li_{10}GeP_2S_{12}$/$LiCoO_2$@$LiNbO_3$ demonstrates good reversibility and narrow overpotentials even after 96 cycles (Fig. 6b). As shown in Fig. 6c, compared with rapid capacity decay for Li/$Li_{10}GeP_2S_{12}$/$LiCoO_2$@$LiNbO_3$ cell, the Li@$LiAlO_2$/$Li_{10}GeP_2S_{12}$/$LiCoO_2$@$LiNbO_3$ cell shows much improved cyclic stability for 96 cycles with a high reversible capacity of 115 mAh g^{-1} and capacity retention of 89%. Fig. 6d shows the excellent rate capabilities of Li@$LiAlO_2$/$Li_{10}GeP_2S_{12}$/$LiCoO_2$@$LiNbO_3$ cell, and the reversible capacity are 130, 121, 105 and 83 mAh g^{-1} at 0.1, 0.2, 0.5 and 1.0 C, respectively, indicating a good reversibility of the capacity at a high cycle rate.

We further investigate the impedance of the Li@$LiAlO_2$/$Li_{10}GeP_2S_{12}$/$LiCoO_2$@$LiNbO_3$ and Li/$Li_{10}GeP_2S_{12}$/$LiCoO_2$@$LiNbO_3$ full cells before and after 96 cycles, as demonstrated in Fig. 6e. Before cycling, the Li@$LiAlO_2$/$Li_{10}GeP_2S_{12}$/$LiCoO_2$@$LiNbO_3$ and Li/$Li_{10}GeP_2S_{12}$/$LiCoO_2$@$LiNbO_3$ cells showed small impedance of 40 Ω and 52 Ω, respectively. However, after 96 cycles, compared with the much higher impedance of 1726 Ω for Li/$Li_{10}GeP_2S_{12}$/$LiCoO_2$@$LiNbO_3$ cell, the Li@$LiAlO_2$/$Li_{10}GeP_2S_{12}$/$LiCoO_2$@$LiNbO_3$ cell showed a suppressed increase of impedance to 581 Ω.

According to the above-mentioned results, the improved cyclic stability of the Li@$LiAlO_2$/$Li_{10}GeP_2S_{12}$/$LiCoO_2$@$LiNbO_3$ cell and its corresponding suppressed increase of impedance further indicate the good protection provided by the $LiAlO_2$ layer on the $Li_{10}GeP_2S_{12}$/lithium metal interface. As illustrated in Fig 7, the $Li_{10}GeP_2S_{12}$/lithium metal interface is prone to the formation of cracks and by-products, such as Li_2S, Li_3P and Li-Ge alloy. In comparison, the $LiAlO_2$ coating layer can greatly reduce the side reaction and formation of by-products on the $Li_{10}GeP_2S_{12}$/lithium metal interface (Fig. 7) while maintaining a good lithium ion conductivity. Also, the good cyclic performance should be benefited from the high mechanic strength and uniform formation of the dense $LiAlO_2$ layer by the magnetic sputtering technique.

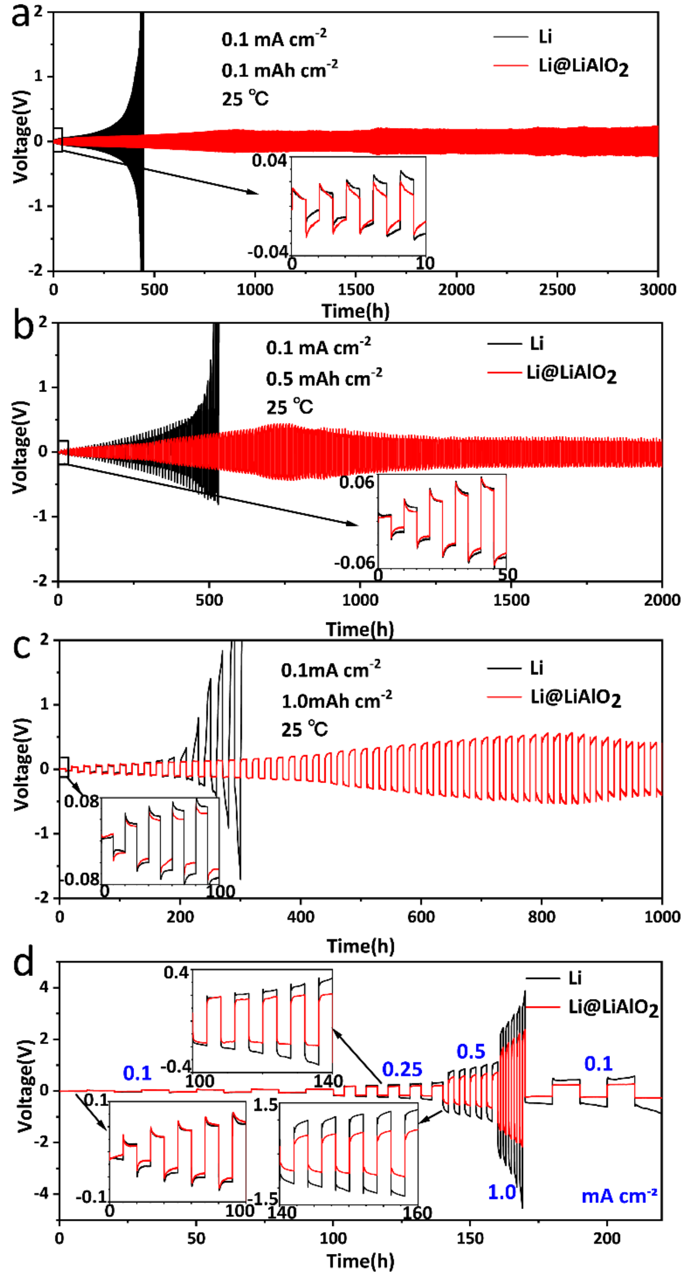

Fig. 5. Cyclic stability of Li@$LiAlO_2$/$Li_{10}GeP_2S_{12}$/Li@$LiAlO_2$ and Li/$Li_{10}GeP_2S_{12}$/Li symmetric cells at (a) 0.1 mAh cm^{-2}, (b) 0.5 mAh cm^{-2} and (c) 1.0 mAh cm^{-2} under current density of 0.1 mA cm^{-2}. (d) Rate capabilities of Li@$LiAlO_2$/$Li_{10}GeP_2S_{12}$/Li@$LiAlO_2$ and Li/$Li_{10}GeP_2S_{12}$/Li symmetric cells at 0.1, 0.25, 0.5 and 1.0 mA cm^{-2}, respectively.

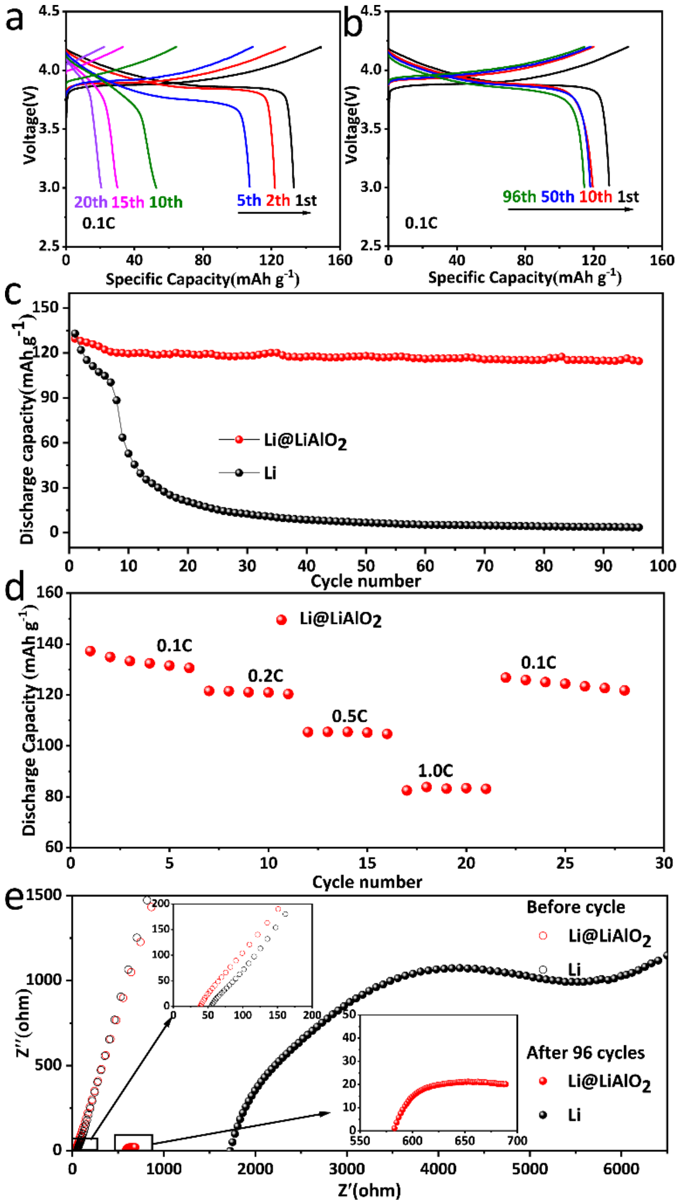

Fig. 6. Charge and discharge curves of (a) Li/$Li_{10}GeP_2S_{12}$/$LiCoO_2$@$LiNbO_3$ and (b) Li@$LiAlO_2$/$Li_{10}GeP_2S_{12}$/$LiCoO_2$@$LiNbO_3$ cell. (c) Cyclic performances of Li/$Li_{10}GeP_2S_{12}$/$LiCoO_2$@$LiNbO_3$ and Li@$LiAlO_2$/$Li_{10}GeP_2S_{12}$/$LiCoO_2$@$LiNbO_3$ cell at 0.1 C under 25 ^{o}C. (d) Rate performances of the Li@$LiAlO_2$/$Li_{10}GeP_2S_{12}$/$LiCoO_2$@$LiNbO_3$ cell. (e) The impedance of the Li/$Li_{10}GeP_2S_{12}$/$LiCoO_2$@$LiNbO_3$ and Li@$LiAlO_2$/$Li_{10}GeP_2S_{12}$/$LiCoO_2$@$LiNbO_3$ cell before and after cycling.

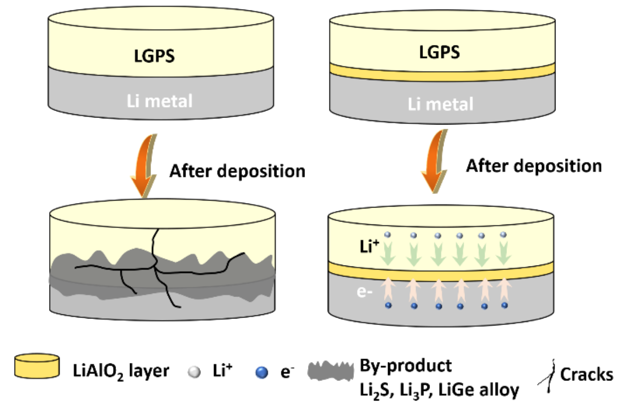

Fig. 7. Proposed interfacial evolution of Li and Li@$LiAlO_2$ negative electrode with $Li_{10}GeP_2S_{12}$ after deposition.

4. CONCLUSIONS

A dense and uniform $LiAlO_2$ layer with high mechanic strength was successfully fabricated on the surface of lithium metal through magnetic sputtering method. The lithium ion conducting but electron insulating $LiAlO_2$ layer could effectively suppress interface side reactions and greatly improve the interface stablity between lithium metal and $Li_{10}GeP_2S_{12}$. By employing the Li@$LiAlO_2$ as electrode, the Li@$LiAlO_2$/$Li_{10}GeP_2S_{12}$/Li@$LiAlO_2$ symmetric cells were able to stably cycle for up to 3000 h with a low overpotential of 200 mV at 0.1 mA cm^{-2} and 0.1 mAh cm^{-2}. The Li@$LiAlO_2$/$Li_{10}GeP_2S_{12}$/$LiCoO_2$@$LiNbO_3$ full cells showed good stability for 96 cycles with a high reversible capacity of 115 mAh g^{-1} at 0.1 C, and good rate capabilities with capacities of 130, 121, 105 and 83 mAh g^{-1} at 0.1, 0.2, 0.5 and 1.0 C, respectively, indicating a good reversibility of the capacity at a high cycle rate. In conclusion, the good performance of $LiAlO_2$ modified $Li_{10}GeP_2S_{12}$-based solid-state lithium batteries shown in this work will enable the better use of $Li_{10}GeP_2S_{12}$ with high ionic conductivity (1.2×10^{-2} S cm^{-1}) and facilitate the further development of all-solid-state lithium batteries.

ACKNOWLEDGEMENT

The work was supported by the National Natural Science Foundation of China (Grant no. U1964205, 51872303, 51902321), Ningbo S&T Innovation 2025 Major Special Programme (Grant No. 2019B10044, 2021Z122), Zhejiang Provincial Key R&D Program of China (Grant No. 2022C01072), Youth Innovation Promotion Association CAS (Y2021080), Zhejiang Provincial Department of Science and Technology (2020E10018), Ningbo Municipal Key Laboratory on

Clean Energy Conversion Technologies (2014A22010) and Ningbo Natural Science Foundation Programme (Grant No. 2021J186).

REFERENCE

1. Grande, L., et al., The lithium/air battery: still an emerging system or a practical reality? Adv Mater, 2015. 27(5): p. 784-800.
2. C, E.E., Lithium batteries ： To the Limits of Lithium. Nature 2015. 526(7575): p. 93-95.
3. Zhao, Y., et al., A promising PEO/LAGP hybrid electrolyte prepared by a simple method for all-solid-state lithium batteries. Solid State Ionics, 2016. 295(Supplement C): p. 65-71.
4. Tarascon J M, A.M., Issues and challenges facing rechargeable lithium batteries. Nture, 2001. 414(6861): p. 359-367.
5. Li, Y., et al., Garnet Electrolyte with an Ultralow Interfacial Resistance for Li-Metal Batteries. J Am Chem Soc, 2018. 140(20): p. 6448-6455.
6. Guo, Y., H. Li, and T. Zhai, Reviving Lithium-Metal Anodes for Next-Generation High-Energy Batteries. Adv Mater, 2017. 29(29).
7. Lin, D., Y. Liu, and Y. Cui, Reviving the lithium metal anode for high-energy batteries. Nat Nanotechnol, 2017. 12(3): p. 194-206.
8. Wu, F., et al., “Liquid-in-Solid” and “Solid-in-Liquid” Electrolytes with High Rate Capacity and Long Cycling Life for Lithium-Ion Batteries. Chemistry of Materials, 2016. 28(3): p. 848-856.
9. Peng, H.J., et al., Janus Separator of Polypropylene-Supported Cellular Graphene Framework for Sulfur Cathodes with High Utilization in Lithium-Sulfur Batteries. Adv Sci (Weinh), 2016. 3(1): p. 1500268.
10. Bruce, P.G., et al., Li-O_2 and Li-S batteries with high energy storage. Nat Mater, 2011. 11(1): p. 19-29.
11. Zhao, B., et al., Asymmetric double-layer composite electrolyte with enhanced ionic conductivity and interface stability for all-solid-state lithium metal batteries. Chinese Chemical Letters, 2021. 32(1): p. 125-131.
12. Wu, J., et al., All-Solid-State Lithium Batteries with Sulfide Electrolytes and Oxide Cathodes. Electrochemical Energy Reviews, 2020. 4(1): p. 101-135.
13. Ye, L. and X. Li, A dynamic stability design strategy for lithium metal solid state batteries. Nature, 2021. 593(7858): p. 218-222.
14. Kamaya, N., et al., A lithium superionic conductor. Nat Mater, 2011. 10(9): p. 682-6.
15. Chen, B., et al., An insight into intrinsic interfacial properties between Li metals and $Li_{10}GeP_2S_{12}$ solid electrolytes. Phys Chem Chem Phys, 2017. 19(46): p. 31436-31442.
16. Shi, Y., et al., Surface Engineered Li Metal Anode for All‐Solid‐State Lithium Metal Batteries with High Capacity. ChemElectroChem, 2021. 8(2): p. 386-389.
17. Li, M., et al., In Situ Formed Li-Ag Alloy Interface Enables $Li_{10}GeP_2S_{12}$-Based All-Solid-State Lithium Batteries. ACS Appl Mater Interfaces, 2021. 13(42): p. 50076-50082.
18. Liu, S., et al., Inducing uniform lithium nucleation by integrated lithium-rich li-in anode with lithiophilic 3D framework. Energy Storage Materials, 2020. 33: p. 423-431.
19. Jiang, Y., et al., $Li_{4.4}Sn$ encapsulated in hollow graphene spheres for stable Li metal anodes without dendrite formation for long cycle-life of lithium batteries. Nano Energy, 2020. 70.
20. Song, X., et al., A lattice-matched interface between in situ/artificial SEIs inhibiting SEI decomposition for enhanced lithium storage. Journal of Materials Chemistry A, 2020. 8(22): p. 11165-11176.
21. Monroe, C. and J. Newman, The Impact of Elastic Deformation on Deposition Kinetics at Lithium/Polymer Interfaces. Journal of The Electrochemical Society, 2005. 152(2).
22. Cheng, X.B., et al., Dendrite-free nanostructured anode: entrapment of lithium in a 3D fibrous matrix for ultra-stable lithium-sulfur batteries. Small, 2014. 10(21): p. 4257-63.
23. Ma, Y., et al., In situ formation of a Li–Sn alloy protected layer for inducing lateral growth of dendrites. Journal of Materials Chemistry A, 2020. 8(44): p. 23574-23579.